they cross the vertical dotted lines. The first step of the calculation consists of "pinching" together the pairs of lines (l, l') and (j_r, j_r), as (j_1, j_2) are pinched in Eq. (4.26) of Ref. 4. Note that the existence of open lines in Fig. 5(a) prevents application of (4.28) of Ref. 4, just as the existence of a dotted line does in (4.26) of Ref. 4. Figure 5(b) shows the result of the double pinching obtained using also our (12) and its representation in Fig. 3. Here and in the following we represent implicitly by the use of heavy lines some of the factors $[j]$ which appear explicitly in the Briggs equations.

At this point the central block of Fig. 5(b), which contains the scattering operators, is connected to the rest by two lines only. We can then apply (4.28) of Ref. 4 in which α represents our central block and α' all the rest; (k, k') correspond to (j_1, j_2). The result is represented by Fig. 5(c), where the closed diagram on the right has to be reduced further.

This final reduction is achieved in two steps as shown in Fig. 5(d). The first step consists of pinching the (j_1, j_2) lines into a single j_t line, applying (4.26) of Ref. 4. The second step consists of a twofold application of (4.30) of Ref. 4 in which one "pinches off" a set of three lines, namely, (j_r, j_t, l) in one case and (j_r, j_t, l') in the other where they intersect the dotted lines.

The resulting 6-j coefficient [e.g., (4.20) of Ref. 4] and $2j_t + 1$ factor are included in the function $\Theta(j_t; j_r m_r, l l'; \theta)$ with the other elements of the diagram. The two remaining blocks represent the $\bar{S}(j_t)$ and $\bar{S}^\dagger(j_t)$ invariant matrix elements on the right-hand side of (14).

*Work supported in part by U. S. Atomic Energy Commission under Contract No. C00-1674-57, and in part by Advanced Research Projects Agency under Contract No. DAHC 15-67-C 0220 Research.

[1]See, e.g., (a) U. Fano, Nuovo Cimento 5, 1358 (1957); and Natl. Bur. Std. (U.S.) Tech. Note No. 83 (1960) (unpublished); (b) U. Fano and G. Racah, *Irreducible Tensorial Sets* (Academic, New York, 1959), p. 114; (c) E. S. Chang and A. Temkin, Phys. Rev. Letters 23, 399 (1969); J. Phys. Soc. Japan 29, 172 (1970). A quantum number j_t has also been introduced as a dummy variable without explicit physical meaning by (d) A. D. Buckingham, B. J. Orr, and J. M. Sichel, Phil. Trans. Roy. Soc. London A268, 147 (1970).

[2]Dan Dill, this issue, Phys. Rev. A 6, 185 (1972).

[3]C. N. Yang, Phys. Rev. 74, 764 (1948).

[4]John S. Briggs, Rev. Mod. Phys. 43, 189 (1971).

[5]M. Rotenberg, R. Bivins, N. Metropolis, and J. K. Wooten, Jr., *The 3-j and 6-j Symbols* (The Technology Press, Cambridge, Mass., 1959), Eq. (2.19).

[6]See, e.g., Ref. 5, Eq. (1.43).

[7]See, e.g., Ref. 5, Eq. (2.20).

[8]See, e.g., F. J. Blatt and V. Weisskopf, *Theoretical Nuclear Physics* (Wiley, New York, 1952), pp. 317–324 and 517–521. An incident-plane-wave state, representing the flux of one particle per second per unit area and expanded in spherical states $|j_r m_r\rangle$ with the values of m_r appropriate to its polarization, has expansion coefficients equal to $\pi^{1/2}(2j_r+1)^{1/2}\lambda_r$. That is, the ingoing flux of the j_rth component equals the flux $\pi(2j_r+1)\lambda_r^2$ which hits a ring target with outer radius $(j_r+1)\lambda_r$ and inner radius $j_r\lambda_r$.

[9]See, e.g., *Raman Spectroscopy, Theory and Practice*, edited by H. A. Szymanski (Plenum, New York, 1967), p. 10ff.

[10]The factors $Q(j \equiv j_t)$ given in Ref. 1(d) are specific examples of Eq. (25).

[11]For specific examples of the general result (26) see, e.g., Ref. 1(c) for the case of electron-molecule scattering, and also, e.g., J. C. Tully, R. S. Berry, and B. J. Dalton, Phys. Rev. 176, 95 (1968) for the case of molecular photoionization.

PHYSICAL REVIEW A VOLUME 6, NUMBER 1 JULY 1972

Electron Excitation of the Sodium *D* Lines*

E. A. Enemark† and Alan Gallagher‡
Joint Institute for Laboratory Astrophysics, University of Colorado, Boulder, Colorado 80302
(Received 7 February 1972)

The electron excitation of the sodium resonance lines (*D* lines) has been measured in the energy range from threshold to 1000 eV. The electron-beam full width at half-maximum was $\sim \frac{1}{3}$ eV, and the sodium-beam optical depth was small and varied. After correction for minor cascade contributions and the measured polarization, the excitation function has been normalized to the Born theory in a high-energy limit where the energy dependence converges to the theoretical behavior. The resulting normalized cross section and the polarization are in excellent agreement with recent close-coupling calculations for the energy region from threshold to 5 eV.

I. INTRODUCTION

Despite the relatively simple electronic structure of sodium, various theoretical calculations of the electron excitation cross section for the 3*s*-3*p* transition have differed considerably.[1] Pre-

vious experimental determinations of this cross section for excitation of the *D* lines (5890 and 5896 Å), have failed to clarify the problem because of their own disagreement.[2-6] Yet this cross section, particularly in the threshold region, is important for the understanding of the formation of the *D* lines in the sun[7] and a variety of other plasmas, such as lamps. Also the entire energy dependence of the cross section is of interest as a nonrelativistic Born-regime test and an extension of calculation techniques to heavy but not too complicated atoms. The review by Moiseiwitsch and Smith[1] (in particular pp. 266–68 and 309–13) illustrates the situation as of 1968.

Most calculations of the cross section have been extensions of the Bethe or first Born approximations (Ref. 1, pp. 266–267). These differ not only in magnitude but also in shape of the cross section as a function of energy (see Fig. 38 of Ref. 1). Close-coupling calculations by Barnes *et al.*[8] and by Karule and Peterkop[9] unfortunately appear to disagree. However, recent close-coupling calculations by Korff *et al.*[10] and by Moores and Norcross[11] indicate agreement with the results of Ref. 9. A model proposed by Vainshtein *et al.*[12] which attempts empirically to include the polarizability of the sodium atom, gives still another cross section.

The experimental results as of 1968 which gave magnitudes to this cross section were those of Christoph[2] and Zapesochnyĭ and co-workers.[3-6] These differ by roughly a factor of 2. Moiseiwitsch and Smith have suggested one possibility for this difference, but there are actually a variety of issues (discussed later) which detract from each measurement. One point of interest in the measurement of Ref. 4 is that even up to 150 eV, roughly 70 times threshold, the excitation function decreases much more gradually than the high-energy Bethe or first Born form of $(\ln E)/E$. (Throughout this paper we use the terminology as defined by Moiseiwitsch and Smith in the discussion starting on p. 278 of their review; the cross section is derived from the apparent excitation function after polarization and cascade corrections have been applied.) This indicates either failure to enter the Bethe regime because of insufficient energy, or experimental error; the effect of cascade contributions to the excitation function should be a more rapid decrease than $(\ln E)/E$.

We report here a measurement of the cross sections and polarization over an energy range extending from threshold (2.1 eV) to 1000 eV. This was accomplished by measuring the relative apparent excitation function over this energy range and applying the appropriate polarization and cascade corrections. Using Born normalization in a region where the relative cross sections fit the predicted Born shape, an absolute magnitude was assigned. Care was taken to eliminate or minimize several possible instrumental and systematic effects which might lead to experimental error; of importance for a later discussion is the fact that these measurements were performed under optically thin conditions. One result of this experiment would be to learn at what energy Born theory predicted the correct cross section; this is of obvious interest to experimentalists and theorists alike.

In addition to being a necessary correction for the cross-section evaluation, the polarization of the resonance radiation observed at right angles to the incident electron beam is itself an interesting quantity. (a) There is a simple prediction for the threshold and infinite energy values for the polarization.[13] Measurements of the sodium resonance radiation in the region a few eV above threshold have been extrapolated smoothly to the threshold prediction.[14] (On the other hand, measurements in helium have indicated that this procedure may often apply only in a very limited range above threshold.) No measurements have yet been reported for the polarization of electron excitation at high energies. (b) Since the Born approximation and other calculations predict polarizations as well as cross sections and experimental errors in polarization measurements are often independent of those in cross-section evaluations, the determination of the resonance radiation polarization is a valuable independent test of theory.

Cascade corrections for both the cross section and the polarization could be estimated from previous work.[4] Fortunately, because of the strong transition probability for this resonance excitation, these cascade corrections were small and uncertainty in the correction causes a much smaller uncertainty in the direct excitation cross section and polarization of the resonance radiation.

II. APPARATUS

In a crossed-beam apparatus the electron and sodium beams intersected at right angles and the observations of the resonance radiation (5890–5896 Å) were made along the third orthogonal axis. Figures 1 and 2 show diagrams of the apparatus in the plane of the sodium beam and the observation axis, and in the plane of the electron and sodium beams. The vacuum chamber evacuated by an ion pump had an operating pressure of 3×10^{-9} Torr.

The measured quantities in this experiment were the relative apparent excitation function given by

$$I(90^\circ) = (I_\parallel + I_\perp)/i \ ,$$

where $I_{\parallel,\perp}$ is the radiation intensity polarized parallel, perpendicular to the electron beam axis and i is the total electron current passing through the sodium beam; the polarization P_m given by

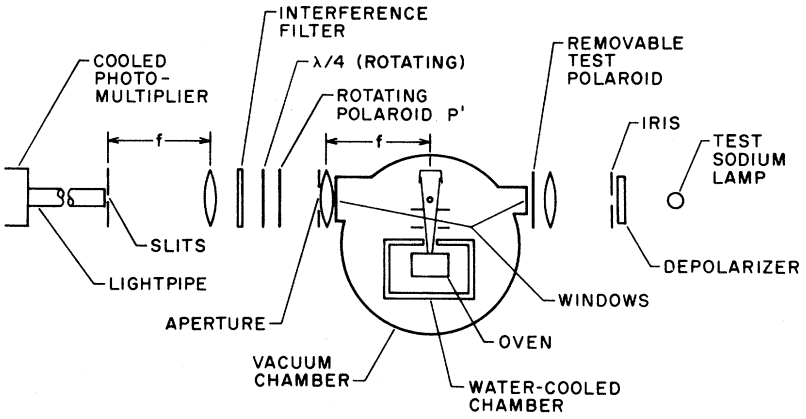

FIG. 1. Diagram of the apparatus in plane of the sodium beam and observation axes. The focal lengths of the two lenses in the detection optics are 4 in., which roughly sets the scale of the diagram.

$$P_m = (I_{\parallel} - I_{\perp})/(I_{\parallel} + I_{\perp}) \times 100\% \ .$$

The distinction between the measured polarization P_m and the actual polarization P of the resonance radiation will be explained later. The manner in which $I(90°)$ and P_m were measured is as follows: The Polaroid in Fig. 1 was rotated at 5 Hz and the 10-Hz modulated portion of the transmitted radiation, which was proportional to $I_{\parallel} - I_{\perp}$, was detected with a lock-in. (The Polaroid rotated about the optic axis so that possible dust and Polaroid inhomogeneities would not cause spurious modulations.) The quantity $(I_{\parallel} + I_{\perp})$ was proportional to the time-averaged output of the photomultiplier. The polarization was proportional to the ratio of these two signals; calibration was attained by passing a 100% polarized signal from a sodium lamp (see Fig. 1) through the detection system and evaluating the ratio.

A. Electron Gun

The basic design criterion for the electron gun was to produce a focused electron beam at a fixed position within the interaction region with a maximum convergence half-angle of 0.1 rad at energies from 1.5 to 1000 eV. The convergence half-angle was restricted in order to maintain corrections to the measured polarization, owing to nonparallel electron trajectories, at about 1% of the measured polarization.[15]

The construction of the electron gun is illustrated in Fig. 2. The gun was designed to operate with the tetrode source filling the fixed field-free apertures of elements A2 and A2′ with electrons. These apertures were then imaged by the variable ratio lens into the interaction region with the correct maximum convergence angle. Aperture A2 was imaged inside the sodium beam while A2′ was imaged beyond. Apertures 1 and 2 bounding the field-free interaction region insured that any electron passing through the interaction region and into the Faraday cup had a maximum convergence half-angle of $(D_1 + D_2)/2L$, which for $D_1 = D_2 = 4$ mm and $L = 40$ mm is 0.1 rad. Appropriate focusing minimized the currents to these apertures, thereby helping to prevent reflected primary and possible secondary electrons from these apertures from passing through the interaction region, and also guaranteeing the required convergence angle. At energies above 12 eV the current to aperture 2 was less than 1% of the total gun current and that to aperture 1 was much smaller. At lower energies these currents did become appreciable, that to aperture 1 increasing to as much as 10% of the total at 2.0 eV, and that to aperture 2 varying from 5% of the total at 10.5 eV to as much as 44% of the total at 2.0 eV. Before actual data taking a third aperture was placed in the interaction region to check that the electron-beam diameter was always smaller than the expected 2 mm. We discuss later the verification that all electrons passing through aperture 1 passed through the sodium beam in the observed region.

The total current passing through the interaction region was evaluated by summing the currents to the Faraday cup, analyzer, and aperture 2 which was constructed as illustrated in Fig. 2 in order to improve current collection. Biasing these collectors positively indicated few secondary electrons within the interaction region. Only at low energies (< 6 eV) was a change greater than 0.1% of the measured current found with positive biasing, with a maximum change of about 4% at 2 eV. (Element V of the electron gun always decelerated electrons from A2′ thereby preventing most secondaries that might be generated at apertures A2 and A2′ from entering the interaction region.) Corrections and error estimates for these current changes were applied where required.

The total current of the electron gun was limited to reduce space-charge effects. Using the appropriate equations from Ref. 16, the maximum potential difference from the walls of the interaction chamber to the center of the electron beam was less than $0.005E$ at all energies (E). (Typical

currents were $0.1E^{3/2}$ μA below 60 eV and 50 μA above.)

The interaction chamber, Faraday cup, and surrounding components were made of materials with similar work functions[17] and were coated with vacuum-baked Aquadag. The magnetic fields within the vacuum chamber due to the earth's field were kept small by means of magnetic shielding. The magnetic field component transverse to the electron-beam axis was less than 20 mG along the entire length of the gun and less than 12 mG in the interaction region. The field component parallel to the electron beam axis was less than 40 mG. All components made of stainless steel were demagnetized when necessary.

B. Sodium Oven

The stainless-steel oven employed a nine-hole effuser (3×3 square array, each hole 0.75 mm in diam and 5 mm deep with ~1.1 mm between centers). The effuser was at a higher temperature than the sodium reservoir; this prevented clogging of the effuser, and reduced the sodium dimer concentration in the beam. Using data from Lapp and Harris,[18] this dimer concentration was estimated to be less than 0.03% and therefore neglected in this experiment. The sodium purity was specified as better than 0.9999 by the supplier. Magnetic fields in the interaction region due to oven heater currents were estimated to be less than 1 mG.

The sodium beam was shaped by the square effuser and a square aperture (3.5×3.5 mm) just outside the interaction region, and was collected by a liquid-nitrogen-cooled copper honeycomb (Fig. 2). Observation of the resonance radiation from the interaction region verified the anticipated constant sodium density over an approximately 3.3 mm length along the direction of the electron beam, and this was assumed to be the case along the observation axis also.

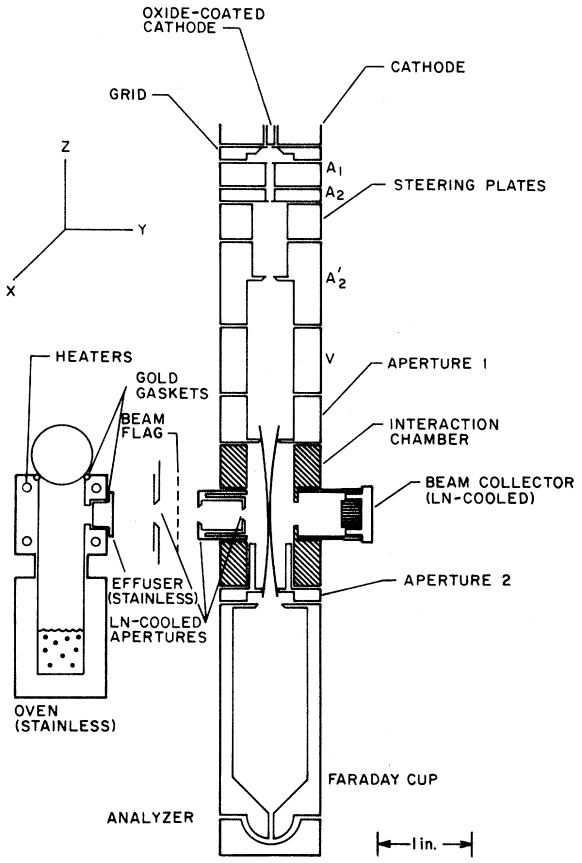

FIG. 2. Scale diagram of the electron gun and sodium oven in plane formed by electron and sodium beams. The tetrode of the electron gun consisted of the cathode, grid, A_1, and A_2 elements. The variable ratio lens was formed by elements A_2', V, and Aperture 1. A_2 and A_2' were at the same potential. The interaction chamber, aperture 1, Faraday cup, and aperture 2 are at ground potential. The lines within the interaction region indicate roughly the design shape of the electron beam (LN stands for liquid nitrogen).

C. Detection System and Instrumental Polarization

The $f/2.4$ optics system used in the detection apparatus is illustrated in Fig. 1. Unless normally incident, radiation will in general experience a polarization change upon transmission from one refractive medium to another. The sodium resonance line polarization is typically only a few percent so all the elements of the optics system were carefully aligned with a laser to be centered on and perpendicular to the optic axis, which was normal to the observation window. With the interaction region in the focal plane of the first lens, the signal radiation was nearly parallel to the optic axis between the lenses, thereby making insignificant the angular shift of the interference filter transmission (40-Å half-width bandpass and 10^4 rejection outside the bandpass).

The rotating quarter-wave plate behind the rotating Polaroid (see Fig. 1) was adjusted to circularly polarize (within 10%) the linearly polarized light from the Polaroid. The effect was to negate possible changes in the relative intensities of $I_{\parallel}$ and $I_{\perp}$ due to reflections off the slit edges in front of the lightpipe, possible transmission differences of the lightpipe for the two polarization directions, and any other possible polarization-dependent measurement effects. The ratio of the Polaroid transmission coefficients was $k_{\parallel}/k_{\perp} \approx 10^4$ and no correction was used for the finite $k_{\perp}$.

The slits used to define the part of the interaction region observed (4×5 mm) by the detection system were imaged on the plane of the electron and sodium beams. The horizontal edges of the slit were set

slightly above and below the region of constant sodium-beam density, blocking roughly 10% of the total beam. The vertical edges were adjusted so that the entire electron beam was observed. The surfaces of the interaction chamber were outside the field of view of the optics. Thus, radiation reflecting off these surfaces, and experiencing possible polarization changes, did not enter the detection optics.

The quartz lightpipe served two functions: First, it acted as a transparent thermal insulator between the room and the photomultiplier which was cooled to about $-25\,^{\circ}$C. Second, the lightpipe was a very efficient means of averaging the signal over the surface of the photocathode. Because the lightpipe was 1 cm in diam and 15 cm long, $f/2.4$ radiation experienced up to three internal reflections within the lightpipe before striking the cathode. This effectively averaged over regions of the cathode with possibly varying sensitivity. The photomultiplier had an S-20 response.

Checks of the instrumental polarization of the detection system were made using a sodium resonance line source placed outside the vacuum chamber (see Fig. 1). The source consisted of a small iris behind which was a "depolarizer" illuminated by a sodium lamp (see Fig. 1). The depolarizer consisted of a 6-mm-thick sheet of Teflon followed by an etched piece of glass with a coating of MgO crystals on the final surface. These crystals averaged over all surface orientations thereby preventing any polarization due to transmission effects. The iris was imaged into the interaction chamber, care being taken to prevent reflection of this light off several surfaces within the chamber. Polarization magnitudes of about 0.1% were obtained, but these were attributed to the test optics rather than to the detection optics. Nonzero polarizations could arise from reflection from the iris edge and transmission through the test window which was about 3° from being perpendicular to the optic axis. Instrumental polarization of the detection system was separately measured by placing the depolarizer inside the vacuum chamber at the position of the interaction region. The result was $(0.00 \pm 0.006)\%$. The 3° tilt of the test window was expected to produce a polarization of magnitude $\sim 0.06\%$, so these two results are reasonably consistent. The $(0.00 \pm 0.006)\%$ is the appropriate correction for the experimental data.

Two instrumental effects required that small corrections be applied to the measured polarization P_m. (These corrections were not needed for the 100% polarization calibration or the instrumental polarization determination for the detection optics.) The interference filter transmission coefficient for the D_1 line (5896 Å) was 2% greater than that for the D_2 line (5890 Å) and this required a $\frac{2}{3}\%$ of P_m increase to the measured polarization magnitudes at all energies as compared to equal detection efficiencies for the D_1 and D_2 lines.[15] Also, the correction for the solid angle of acceptance of the $f/2.4$ detection optics and the convergence angle of the electron beam was a net increase of 2% of P_m.[15]

III. MEASUREMENTS

The polarization and excitation functions for the unresolved resonance doublet were measured at a number of energies from below threshold (2.1 eV) to about 1000 eV. Several checks were performed to guarantee correct measurement of the polarization and excitation function. These checks along with the measurement techniques and data reduction are discussed in this section.

A. General Checks

Tests for modulated or dc background signals (for instance from the sodium oven, electron gun cathode, ion pump, and motor for the rotating Polaroid), electronic saturations, drifts, and loadings were all satisfactory. Precision (0.1%) attenuators or photoelectron counting techniques were used to compare signal sizes.

The polarization and excitation functions at 100 eV were measured versus the total electron gun current i. As long as the electron beam shape remains the same, space-charge depression remains small, and the electron beam passes through the uniform density portion of the sodium beam; the polarization P_m and the apparent excitation function $I(90^{\circ})$ should remain constant as i is varied. Contrary results would be a strong indication of experimental error. Both P_m and $I(90^{\circ})$ remained constant to within statistics as i was varied a factor of 5; P_m varied a maximum of 4% of P_m, with an rms variation of 1.3% of P_m; $I(90^{\circ})$ varied a maximum of 3%, with an rms variation of 1.3%.

Electron collection efficiency and excitation due to secondary electrons were discussed in Sec. II A. The energy of the electrons was measured by retardation with a hemispherical energy analyzer behind the Faraday cup[19] (see Fig. 2). With energies measured in this way, the analyzer voltage for the position of the threshold of the excitation function shifted with time, starting about 0.4 eV below the true threshold of 2.1 eV and gradually moving to about 1.2 eV below 2.1 eV after about 25 h of beam operation. This shift was essentially linear with total sodium-beam flow. It was attributed to a gradual buildup of a sodium coating in the interaction chamber as sodium was deposited in the liquid-nitrogen-cooled beam collector and to a lesser extent on the interaction chamber walls. (Previously it has been found in a test setup that the probability for thermal sodium atoms sticking to a liquid-nitrogen-cooled copper surface was

significantly less than 1.0.) Sodium has a work function roughly 2 V less than that of Aquadag[17] and so electrons entering the interaction chamber were accelerated by this contact potential change. This manifested itself as a decrease in the apparent excitation function threshold energy.

This explanation was verified in two ways: As mentioned above, the size of the threshold energy shift was correlated with the amount of sodium used. The other check was to heat the interaction chamber to drive sodium off the walls after enough sodium had been used to cause an 0.8-eV shift. As expected this shifted the effective threshold energy back to the value first observed with a clean chamber. The difference between the clean chamber threshold of 1.7 eV and the true threshold of 2.1 eV was attributed to fixed contact potential differences.

B. Electron- and Sodium-Beam Overlap

The apparent electron excitation function signal at a given energy is proportional to the volume integral of $N(x, y, z)\, I(x, y, z)\, S(y, z)$ where the electrons are incident along the z axis, the sodium atoms are incident along the y axis, and the observation direction is along the x axis (see Fig. 2). Here, $N(x, y, z)$ is the sodium-beam density, $I(x, y, z)$ is the electron-current density, and $S(y, z)$ the detector sensitivity. As a first approximation, the sodium beam was to have a constant density for all observed regions traversed by any part of the electron beam at all energies, and the detection system sensitivity was to be uniform over the region observed by the detection optics. If these two design criteria are met, the signal at a given energy reduces to NSi, independent of position in the interaction region. Here we describe checks to determine whether this simplification is valid. (Note that since the polarization is a ratio of intensities, the beam overlap problem does not influence the polarization measurement.)

The position and size of the electron and sodium beams in the yz plane within the interaction volume were mapped by moving slits across the image of the interaction region in front of the photomultiplier lightpipe (see Fig. 1), and recording the output of the photomultiplier as a function of slit position. Figure 3 shows the position and shape of the electron beam at two energies, 2.3 and 100 eV. The shapes of these electron beams are similar but the positions are different. This was attributed to residual magnetic and electric fields and possible focusing effects. The position of the 100-eV beam is characteristic for all energies from 1000 eV down to ~ 25 eV. Below 25 eV, the beam position moved gradually, then rapidly, toward the 2.3-eV position. The 2.0-eV beam was ~ 0.1 mm further shifted.

Figure 3 also shows the position of the slit edges that fixed the width of the observed portion of the interaction region for data collection. It is clear that these positions guaranteed collection of radiation due to the entire electron beam at all energies. Since the sodium $3p$ state lifetime is ~ 16 nsec and the average beam velocity is ~ 4×10^4 cm/sec, directly excited atoms would not leave the field of view before decaying. Also, almost all of the cascading is from the $3d$ and $4s$ states, which decay into $3p$ within the field of view. Centering of the electron beam within the sodium beam in the x direction is discussed below.

A 3.3-mm uniform-umbra region and an approximately 1-mm penumbra was expected for the sodium-beam shape in the x and z directions since the beam defining apertures were square. Measurements of the profile of the sodium-beam excitation along the electron beam (z) direction were consistent with this expected shape. For the data measurements the horizontal slit edges were positioned in the image of the penumbra region, excluding about 10% of the sodium beam. Due to the slow expansion of the sodium beam in the z direction, this excluded percentage increased gradually with y. Combined with the shift of the electron beam along the y direction at low energies, this should cause about a 1% change in detected signal between 2 and 10 eV. The statistical uncertainty in the data in this low-energy region made this an insignificant correction.

The size of the electron beam was shown to be less than 2 mm in diam at all energies as discussed in Sec. II A, and the sodium beam had a uniform-density-umbra region 3.3 mm square in the xz plane which varied slowly along the sodium-beam direction (y axis). To guarantee that the smaller electron beam passed through the umbra portion of the sodium beam at all incident electron energies, two tests were performed: A small metal strip 2.2 mm wide could be inserted into the sodium beam at a position just before the interaction region; this removed the central portion of the beam. With this

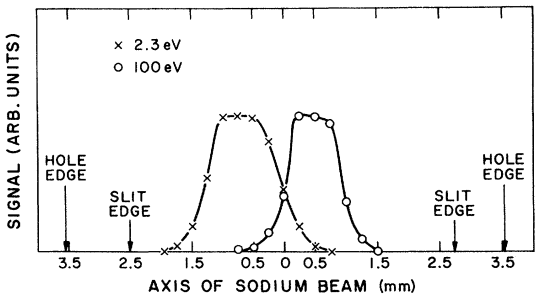

FIG. 3. Position and shape of the 2.3- and 100-eV electron beams in the sodium beam, as measured by scanning the image of the interaction region.

metal strip in position, the excitation signal dropped to zero for all but the lowest electron energies (< 5 eV), indicating the electron beam passed through the center of the sodium beam. As seen in Fig. 3 the low-energy beam was larger, owing possibly to the Coulomb repulsion of the electrons or focusing effects. Although this may indicate that the low-energy beam position was also shifted slightly in the observation (x) direction, it is much less than the y shift shown in Fig. 3.

To be sure the electron beam still passed through the umbra of the sodium beam at these low energies, the 2-mm-diam electron beam at 2.3 eV was moved by means of the steering plates in the electron gun (see Fig. 2) from its original position ~ 0.5 mm in both directions along the observation axis. Less than $\frac{1}{2}$% change in signal level was found so it was concluded that this electron beam still passed through the umbra of the sodium beam.

The question of uniform detection system sensitivity was touched upon in Sec. II C when the averaging property of the photomultiplier lightpipe was described. Also, for a 1-mm movement of the electron beam along the sodium-beam direction away from the oven, the 100-eV signal level decreased by about 1%, consistent with the previous discussion of sodium-beam expansion. This was taken as evidence that the factor $S(y, z)$ was constant to within 1% throughout the interaction region, and it was concluded that the signal at a given energy was proportional to NSi.

C. Sodium Density Dependence

The effect of the sodium-beam density on the polarization and optical excitation function was measured. The 100-eV signal size was used as an index of sodium-beam density. Estimates of the sodium-beam density were made from (i) vapor pressure in the oven and effusive flow relations and (ii) the determined cross section and estimated detection efficiency. Both estimates gave values of a few times 10^{10} atom/cm^3 at the highest densities used in the experiment. Taking into account the less than full Doppler linewidth, due to the beam collimation, this corresponds to an optical depth of about 0.3 along the optic axis for the average path of ~ 0.2 cm through the beam.

Radiation entrapment can affect apparent excitation function measurements when the excited state can decay to more than one lower state (see p. 279 of Ref. 1). Since the transition studied here is from the first excited state to the ground state, no such effect should be expected. A measurable change in the apparent excitation function could occur due to depolarization during radiation diffusion, which changes $I(90°)/I_{tot}$. Polarization data shown below demonstrate that for $E \geq 7$ eV less than 0.6% polarization decrease occurred at the largest beam densities used. This produces a negligible (0.2%) change in Eq. (1). Below 7 eV this increases to 0.5% but is still negligible compared to the experimental uncertainties. Anisotropy of absorption within the sodium beam due to the anisotropic velocity distribution will alter the detected intensity, but by almost the same amount for all electron energies. These expectations were confirmed by an inspection of the excitation function at several N values, which showed no systematic variation.

The magnitude of the polarization $|P_m|$ should decrease as the sodium-beam density N is increased because of radiation entrapment (p. 282 of Ref. 1). This is because polarized radiation, when absorbed and reemitted by similar atoms, is partly depolarized. Two effects cause this depolarization: One a geometrical averaging over directions of radiation propagation, and the other due to disorientation of the electric dipole axis by the electron and nuclear spin interactions. The first process causes a gradual decrease in observed polarization of about 25% per scattering, [20] whereas the latter mechanism is much more effective for complex multiplet structures such as the $3\,^2P$ levels of sodium. Close to 90% of the polarization is lost in each successive scattering of the Na D_2 line. [21] Thus the observed radiation is a combination of polarized radiation from the electron excited atoms and less polarized radiation from successive scatterings, effectively reducing the magnitude of the polarization of the original electron impact radiation.

The effect of radiation entrapment on the magnitude of the polarization is shown in Fig. 4. Here $\ln P_m$ for several energies is plotted versus the sodium-beam density N($N = 200$ corresponds to an estimated beam density of a few times 10^{10} atoms

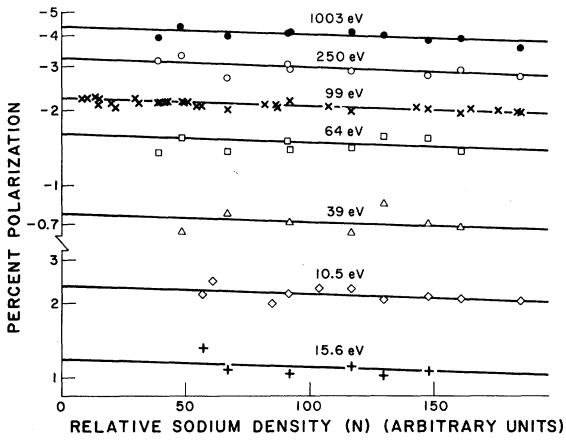

FIG. 4. Polarization of resonance radiation as a function of relative sodium-beam density N for several electron energies. The instrumental corrections discussed in Secs. II A and II C have been applied to the data. The slopes of the fitted lines are required to be equal.

TABLE I. Results for polarization of directly excited sodium resonance radiation.

Energy (eV)	P'_m (%)	P'_m uncertainty (%)	Cascade (%)	P_D (%)	P_D uncertainty (%)	P true direct excitation (%)
1003.0	−4.36	0.06	5.5	−5.0	0.10	−4.39 ± 0.12
802.1	−4.23	0.10	5.5	−4.9	0.11	−4.25 ± 0.15
601.2	−4.01	0.05	5.9	−4.9	0.11	−4.02 ± 0.12
400.4	−3.65	0.07	6.2	−4.7	0.10	−3.65 ± 0.12
249.8	−3.25	0.06	6.8	−4.5	0.10	−3.23 ± 0.12
149.4	−2.75	0.04	7.4	−4.0	0.09	−2.71 ± 0.10
99.2	−2.25	0.03	8.5	−3.3	0.09	−2.22 ± 0.10
63.7	−1.64	0.05	9.6	−2.4	0.06	−1.62 ± 0.08
38.7	−0.79	0.04	12.0	−0.9	0.05	−0.80 ± 0.07
23.8	+0.23	0.04	13.5	+0.9	0.05	+0.16 ± 0.07
15.6	+1.22	0.05	14.7	+2.7	0.09	+1.06 ± 0.10
10.5	+2.38	0.06	15.5	+4.5	0.19	+2.17 ± 0.20
7.0	+3.7	···	16.3	+6.4	0.2	+3.5
5.0	+5.3	···	14.4	+8.0	0.3	+5.2
4.0	+6.4	···	6.3	+9.1	0.3	+6.4
3.0	+8.3	···	0.0	···	···	+8.3
2.5	+10.0	···	0.0	···	···	+10.0

per cm^3 or an effective optical depth of about 0.3). For analysis of the data, a model was assumed which gave the polarization as a function of N as $P(E, N) = P(E, 0)e^{-bN}$. This model assumes that radiation which has been absorbed and reemitted by sodium atoms in the beam is unpolarized, and that the radiative trapping is independent of electron energy. The atomic recoil Doppler shift is small enough to justify this, as are changes in the electron-beam position.

To determine the constant b, the polarization values (corrected for the instrumental effects mentioned in Secs. II A and II C) for several N values were plotted as illustrated for some energies in Fig. 4. A linear least-squares fit, weighted by the standard deviations of the means for individual points, determined the slope and intercept for each $\ln P'_m$-vs-N plot. Assuming that the slope for each set of data should be the same, a weighted average of these computed slopes was found. Fitting this average slope again by the least-squares method to each set of data gave the intercepts listed in column 2 of Table I. Lines of this averaged slope are drawn through the data shown in Fig. 4; inspection of this figure indicates that the assumption of a fixed slope at all energies seems valid. (The differences between the intercepts computed using the average slope and those found using the slopes determined from each set of data averaged about 5% of the intercept.)

This method of correcting the measured polarizations for radiation entrapment was not applied to the data taken at incident energies less than 10 eV. Recall the previous discussion in Sec. II A concerning the shift of the excitation threshold due to sodium deposits on the walls of the interaction chamber. Because of this shift in the electron energy, it was difficult to accumulate several polarization data at a well-defined energy. Since the polarization changes more rapidly as a function of energy in this low-energy region, the individual polarization results were corrected for instrumental effects and radiation trapping and plotted individually. These data will be presented in the next section.

The low-energy apparent-excitation-function data (energy < 12 eV) were also affected by this gradual energy shift. Consequently individual measurements are presented in Sec. IV rather than an average of several points at one energy.

IV. RESULTS

In column 2, Table II, the observed relative apparent excitation function is given. The uncertainties are standard deviations of the mean of the averaged data. These uncertainties also include possible errors introduced by sodium-beam density fluctuations: The density normally varied by less than 5% between successive 100-eV measurements and by less than 15% over several hours.

In order to obtain the cross section from the relative apparent excitation function $I(90°)$, the corrections mentioned in the Introduction for the anisotropy of polarized fluorescence and cascade contributions must be made and a magnitude must be assigned. The polarization anisotropy correction, [22]

$$Q_T = Q_{\text{direct + cascade}} \propto I(90°)\left(\frac{300 - P}{300}\right), \qquad (1)$$

is given in Table II.

Cascading arises when the incident electrons

have sufficient energy to excite the sodium atoms to levels above the $3p$ state. These atoms can decay to the $3p$ state and then to the $3s$ state, emitting the D lines. Cascade effects will also contribute to the measured polarization of the resonance radiation. The maximum cascading appears to be about 16% of the total $3p$-$3s$ fluorescence, and it drops to less than 6% at 1000 eV.

An estimate of the cascade contribution to the apparent excitation function for the $3s$-$3p$ transition can be made using the results of Zapesochnyĭ and Shimon[4] for cross sections to higher states. In addition to the $3s$-$3p$ excitation function, they measured the cross sections for the higher-lying s and d states by observing the intensities on an absolute scale of the radiations corresponding to the various transitions from these higher s and d states to the $3p$ state and normalizing by means of a standard light source. Summing these cross sections should give a good estimate of the total cascade contribution to the apparent excitation function. (Zapesochnyĭ and Shimon worked at high optical depths for the resonance transition only. Possible errors in their $3p$ excitation function due to radiation entrapment will not arise for these other cases.)

Zapesochnyĭ and Shimon measured these cross sections up to 30 eV. We extend their results to 1000 eV by assuming that these dipole-forbidden cross sections decrease with increasing energy as $1/E$, corresponding to the high-energy limit.[23] The sum of the cross sections for the s and d states and extension of these results to 1000 eV are given in Fig. 5 and Table II. From the results of Zapesochnyĭ and Shimon we find that ~ 20% of the cascade is from the s states and ~ 80% from the d states with ~ 75% from the $3d$ state in particular. The $3s$-$3d$ cross section has been calculated at 4 and 5 eV in Refs. 11 and at 17 and 23 eV in Ref. 10 using close-coupling techniques. These results along with the $3d$ cross section given by Zapesochnyĭ and Shimon are also given in Fig. 5. The agreement supports the cascade estimates, except at 4 eV where the theory suggests a larger cascade contribution.

It might be asked whether the higher-p states contribute significantly to the cascade. From Ref. 4 the p-state cross sections decrease rapidly with increasing principal quantum number, the $4p$-state cross section being 0.5% of that for the $3p$ state. Also, using the transition probabilities of Ref. 24, ~ $\frac{1}{3}$ of the $4p$ state population decays directly to the ground state. Hence p state contributions to the cascade to the $3p$ state have been neglected.

In order to assign a magnitude to the relative optical excitation function and thus determine the direct cross section we normalize at high energy. We use first Born approximation cross sections for the direct excitation. The Born cross sections

TABLE II. Cross-section data.

Energy (eV)	$R(E)$, relative apparent excitation function	Q_T, relative optical excitation function	Q_C, cascade (πa_0^2)	Q_B, Born cross section (πa_0^2)	Q_T, normalized optical excitation function (πa_0^2)	Q_D, normalized direct cross section (πa_0^2)	Q_D uncertainties cascade statistical (πa_0^2)	
1003.0 ± 0.2	0.154 ± 0.001	0.1560	0.136	2.39	2.526	2.39 ± 0.02	0.00	0.02
802.1 ± 0.2	0.186 ± 0.001	0.1885	0.170	2.88	3.053	2.88 ± 0.03	0.01	0.02
601.2 ± 0.3	0.237 ± 0.001	0.2405	0.226	3.69	3.892	3.67 ± 0.03	0.01	0.02
400.4 ± 0.3	0.334 ± 0.002	0.338	0.340	5.19	5.477	5.14 ± 0.04	0.02	0.03
249.8 ± 0.4	0.492 ± 0.002	0.497	0.55	7.66	8.046	7.50 ± 0.05	0.04	0.03
149.4 ± 0.5	0.736 ± 0.004	0.743	0.91	11.6	12.03	11.1 ± 0.1	0.1	0.07
99.2 ± 0.5	1.000	1.007	1.36	16.1	16.35	15.0 ± 0.2	0.2	...
63.7 ± 0.4	1.34 ± 0.01	1.35	2.1		21.9	19.8 ± 0.4	0.3	0.2
38.7 ± 0.3	1.80 ± 0.01	1.80	3.5		29.2	25.7 ± 0.7	0.6	0.2
23.8 ± 0.3	2.24 ± 0.02	2.24	4.9		36.3	31.4 ± 1.1	1.0	0.3
15.6 ± 0.3	2.52 ± 0.02	2.51	6.0		40.7	34.7 ± 1.4	1.3	0.3
10.5 ± 0.2	2.68 ± 0.02	2.66	6.7		43.1	36.4 ± 1.6	1.5	0.3
7.0 ± 0.1	2.73 ± 0.05	2.69	7.1		43.6	36.5 ± 1.9	1.7	0.8
5.0 ± 0.1	2.59 ± 0.05	2.53	5.9		41.0	35.1 ± 1.6	1.3	0.8
4.0 ± 0.1	2.40 ± 0.05	2.34	2.4		38.0	35.6 ± 0.9	0.1	0.8
3.0 ± 0.1	1.95 ± 0.05	1.90	0		30.8	30.8 ± 1.0	0.6	0.8
2.5 ± 0.1	1.48 ± 0.05	1.42	0		23.0	23.0 ± 1.0	0.5	0.8

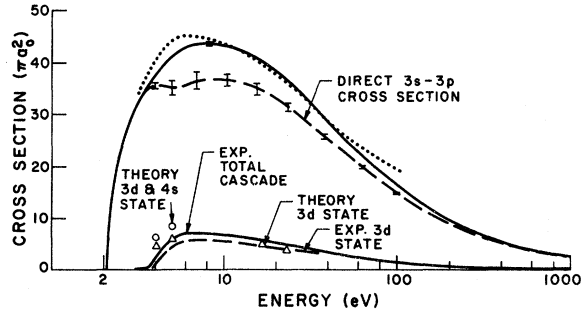

FIG. 5. Normalized direct excitation cross section (dashed) and direct plus cascade cross section (solid) as a function of incident electron energy. The uncertainty bars are relative to the Born normalization at 1000 eV (Fig. 6), and are predominantly due to a ± 35% uncertainty allowed for in the experimental cascade cross section. The experimental cascade cross section is from the measurement of Ref. 4 extended from 30 to 1000 eV by assuming an E^{-1} dependence. The $3d$ state cross section of Ref. 4, which is responsible for most of the cascade, is compared to the calculation of Ref. 10 in the neighborhood of 20 eV and to Ref. 11 at 4 and 5 eV. The relative apparent excitation function (direct plus cascade cross sections without a minor polarization correction) from Ref. 26 is shown arbitrarily normalized for comparison to our data (dots). This is not extended to threshold to avoid confusing overlap; some minor structure was found, but the overall pattern essentialy agrees with the present results.

(given in column 5 of Table II) were taken from Karule and Peterkop.[9] These were extended to 1000 eV using an oscillator strength[24] of 0.98 and the appropriate expression from Geltman.[23] To these we add the cascade cross section in Fig. 5 to obtain a total excitation function, normalize our relative excitation function to this at 1000 eV, then subtract the cascade cross section to obtain the direct component (Table II). This is shown as QE vs $\log_{10}E$ in Fig. 6. Note that uncertainty in cascade cross section at 1000 eV has no effect on the resulting 1000-eV direct cross section. Whatever cascade value is used, it is just added in and then subtracted back off. This normalized 1000-eV direct cross section does have about ± 3% uncertainty due to uncertainty in the optical oscillator strength.[24] If new information comes to light on this oscillator strength, our cross-section scale should be correspondingly adjusted. We have not included this uncertainty in the bars of Fig. 5 since it is a correlated uncertainty, which scales all points equally.

A ± 35% uncertainty in the cascade cross section has been allowed for in column 8 of Table II. This size uncertainty is given in Ref. 4, and in view of the agreement with the $3d$ state calculations of Ref. 10 it appears sufficient. The resulting uncertainty in our direct cross section is much less than 35% of the cascade cross section, because the cascade is added in before normalization at 1000 eV then subtracted back off to obtain the experimental direct cross section. Only the difference between the energy dependence of the cascade and total excitation causes a net uncertainty, i. e.,

$$Q_{\text{direct}}(E) = R_T(E)\,Q_B(1000\text{ eV}) + Q_C(1000\text{ eV})[R_T(E) - R_C(E)],$$

where $R_T(E) = I(E)/I(1000\text{ eV})$ is the experimental optical excitation function and $R_C(E) = Q_{\text{cascade}}(E)/Q_{\text{cascade}}(1000\text{ eV})$. The cascade from higher-P states is proportional to $(\log_{10}E)/E$ above 100 eV, so this changes the slope of the direct plus cascade line in Fig. 6. Since the total p cascades are estimated at less than 1% of the direct cross section we have not included this. Thus the direct cross sections from 250 to 1000 eV have a relative uncertainty which is just the typically ± ½% uncertainty in $I(90°)$ shown in Table II. As can be seen in Fig. 6, this results in a quite accurate test of the approach to the Born cross section. The fact that the experimental points systematically approach the theoretical slope gives strong support to the accuracy of the measurements and the validity of the Born normalization. This property is independent of the oscillator strength chosen for the Born cross section; a different oscillator strength will simply change the scale of the ordinate of Fig. 6. (Our measurements yield no information regarding the optical oscillator strength.)

The normalized direct cross section at all energies is given in Figs. 5 and 7. The cross sections below 11 eV are derived from the smooth

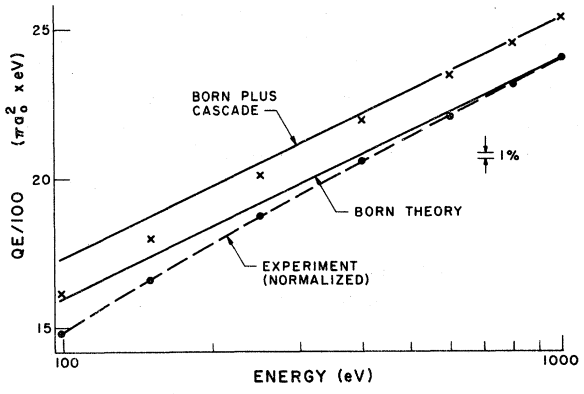

FIG. 6. QE vs $\log_{10}E$ for $E > 100$ eV. The cascade cross section (Fig. 5) is an E^{-1} extrapolation of the data in Ref. 4. The ×'s are the experimental relative excitation function normalized to Born plus cascade at 1000 eV; the dots are obtained from these by subtracting the cascade cross section. Note that changing the size of the cascade raises the ×'s but leaves the dots essentially unchanged; the experimental direct cross section is thereby normalized to the Born theory at 1000 eV.

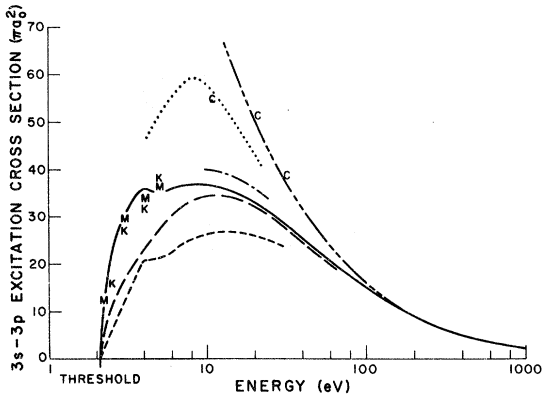

FIG. 7. Comparison of normalized $3s$-$3p$ direct excitation cross section (solid line) with other measurements and calculations. Measurements of Ref. 6 (------); measurements of Ref. 2 (*C*); calculation of Ref. 12 (——); calculation of Ref. 8 (dots); calculation of Ref. 10 (– – –); calculation of Ref. 9 (*K*); calculation of Ref. 11 (*M*); Born cross section from extrapolation of Ref. 9 (– – –). The optical excitation function measurements of Ref. 26 are compared to the present measurements in Fig. 5. The uncertainties in the present measurements are in Table I and Fig. 5.

line drawn through the excitation function data given in Fig. 8. The uncertainties in the energies given in Table II represent contact potential and space-charge effects.

In order to assign uncertainties to these cross sections, we consider the following: One factor to be considered is the uncertainty in $I(90°)$ caused by sodium-beam density fluctuations. These uncertainties are indicated in column 2 of Table II, combined with uncertainties due to statistical fluctuations which, because of the size of the signal, are less than 0.1% for the energies > 10 eV. For energies below 10 eV, an uncertainty can be estimated by examining the scatter of the data about the smooth line fit in Fig. 8. The uncertainty in normalized cross section due to the ± 35% uncertainty in the cascade cross sections is shown in Table II, column 4. Adding these in quadrature gives the net uncertainty in Fig. 5 and in Table II, column 5. The additional ± 3% scale uncertainty due to the optical oscillator strength is not included here.

Other possible systematic effects also cause uncertainties. One important issue is the possible failure to collect all the primary electrons in the electron beam. Electrons entering the Faraday cup may scatter off the walls of the cup and then exit. Biasing the electron collectors positively will not guarantee collection of all elastically scattered electrons because electrostatic fields are conservative. The cup design and biasing and steering tests suggest that this caused negligible error. Another conceivable systematic error could be due to excitation of the sodium beam by secondary electrons coming back out of the Faraday cup and aperture 2. For energies > 10 eV, these lower-energy electrons have a larger excitation cross section; however, we have shown that for energies > 10 eV, the secondary electron contribution to the total electron gun current was less than 0.1%. For lower energies, the secondary electron contribution was no more than 4% at 2.0 eV. Also the solid angle of the sodium beam from the Faraday cup is quite small.

With the knowledge of the percent cascade contribution to the observed signal radiation, the cascade effects on the observed polarization could be evaluated. The polarization of the $3p$ state resonance radiation due to cascade was evaluated in the following way: Assuming unresolved hyperfine structure for the d states[25] and resolved hyperfine structure in the $3p$ state,[13] the method of Percival and Seaton[22] was used to determine the cascade polarization at the $3d$ state threshold (3.6 eV) and at infinite energy. Then assuming a $1/E$ approach to the infinite energy limit because the $3s$-$3d$ transition is dipole forbidden and a 0% polarization at ~ 30 eV by analogy to the direct excitation polarization, a smooth curve could be drawn through the energy range studied here. The results are given in column 3 of Table I. Resonance radiation caused by cascade from the higher s states will be unpolarized. Thus we can find the polarization of the directly excited radiation at each energy by using the approximate relation

$$P_m' = (1 - C_D - C_S)P + C_D P_D , \qquad (2)$$

where P_m' is the measured polarization corrected for instrumental and density effects. $C_{D,S}$ represents the fraction of the $I(90°)$ signal radiation due to cascading from the D and S states, P is the true

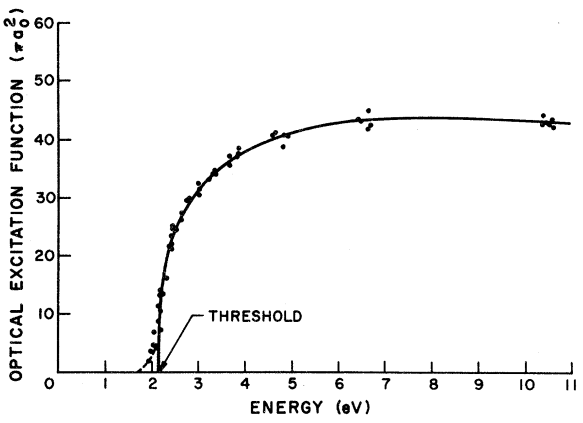

FIG. 8. Normalized optical excitation function in the threshold region. The dashed extension of the solid line fit is due to the ~0.3-eV FWHM electron energy distribution.

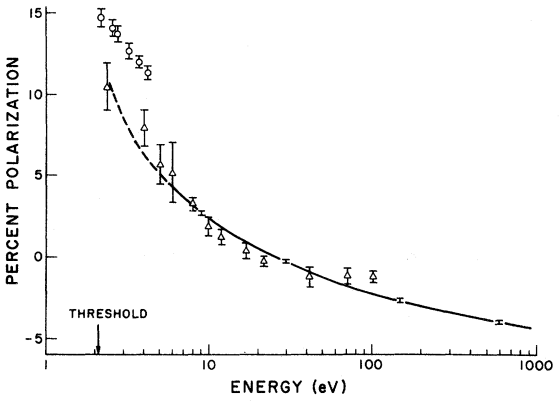

FIG. 9. Measured polarization of resonance radiation due to direct excitation (solid line with dashed extension through the data in Fig. 10). The measurements of Ref. 26 are also shown (triangles) for comparison. Open circles are experimental results of Ref. 14.

polarization of the directly excited resonance radiation, and P_D is the calculated polarization of the resonance radiation due to cascade from the d states. The results are given in the last column of Table I and Figs. 9 and 10. For energies below 10 eV in Fig. 9, the polarizations are taken from the smooth curve in Fig. 10.

The uncertainties in the polarizations for energies above 10 eV were evaluated in the following manner: The statistical uncertainties due to scatter of the polarization data at a given energy about the fitted straight line in Fig. 4 and due to the uncertainty in the slope of the straight line itself were evaluated. Second, using Eq. (2) and ± 35% uncertainties for C_D and C_S and reasonable extremes for P_D, uncertainties in the true polarization P were determined. All these uncertainties are given in Table I, and the final total uncertainty for P was found by adding these estimated uncertainties in quadrature.

Possible systematic errors due to secondary electrons would probably cause the measured polarization to be slightly too positive, because the low-energy polarizations are more positive than high-energy polarizations. However, as discussed previously, secondary electron contributions to the total electron gun current were < 0.1% over most of the energy range.

V. DISCUSSION AND CONCLUSIONS

The purpose of this experiment was to measure the relative apparent electron excitation function and the polarization of the unresolved resonance doublet radiation for the $3s$-$3p$ transition in sodium. Using data from another experiment, with theoretical support, to estimate cascade contributions and normalizing to Born cross sections at high energies, the absolute cross section shown in Fig. 5 was determined. It is important to note that the normalization was a shape, not a point, normalization to Born theory at energies a few hundreds times threshold (see Fig. 6); using the Born cross section at 600 or 800 eV would yield essentially the same results as those found by normalization at 1000 eV.

Some comparison can be made between our cross-section results and several theoretical results which are plotted in Fig. 7. There is good agreement between our results and those of Karule and Peterkop,[9] which is a two-state close-coupling calculation including exchange. Recently, Moores and Norcross[11] have completed a more elaborate four-state close-coupling calculation including exchange in which they have included the two major cascade contributors, the $3d$ and $4s$ states. As seen from Fig. 7, their cross sections are not very different from those of Karule and Peterkop, although they are closer to our results. Good agreement is also found with the three-state ($3s$-$3p$-$3d$) close-coupling (excluding exchange) results of Korff *et al.*[10]; this calculation was an improvement upon the older two-state close-coupling results of Barnes *et al.*[8] The model proposed by Vainshtein *et al.*[12] seems to yield values in good agreement with our results for energies greater than 10 eV. Most other theoretical calculations give larger cross sections (see Fig. 38 of Ref. 1).

Satisfactory agreement is found with the recent experimental results of Gould[26] (Fig. 5). Because Gould used slightly different cascade corrections and normalization which caused ~ 10% differences from our cross-sections results, we have plotted his optical excitation function normalized to ours at 10 eV. The shapes of Gould's and our functions

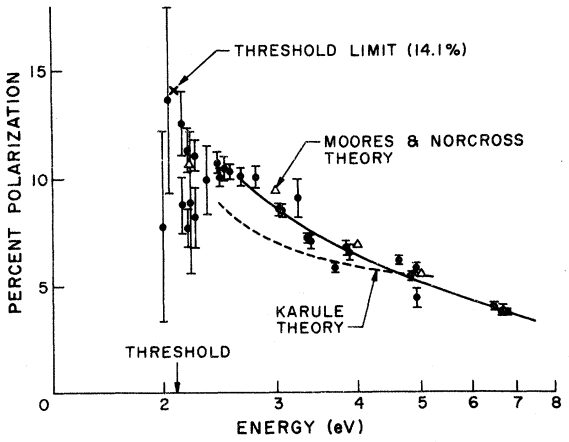

FIG. 10. Resonance radiation polarization near threshold (one standard deviation shown). Experimental results of Ref. 26 are shown in Fig. 9. Dashed line is a smooth curve through four theoretical points of Ref. 9. Solid triangles are calculations of Ref. 11. The expected threshold polarization is shown (Ref. 13).

are similar; especially important for astrophysics is the basic agreement in the threshold region. (Gould's data, taken with greater energy resolution, indicated some structure in the first eV above threshold, which causes some 10–20% difference from our data.)

The experimental results of Christoph[2] and Zapesochnyĭ[6] differ markedly from ours and from each other (Fig. 7). Moiseiwitsch and Smith[1] have proposed that a possible systematic effect due to incorrect sodium density evaluation could affect all of Zapesochnyĭ's cross sections; however this explanation may be insufficient to account for the differences of these experiments. Instead we suspect that the nonresonant transition cross sections from Ref. 4 may well be accurate, but that the Refs. 4 and 6 as well as Christoph's resonant transition cross sections are incorrect due to radiation trapping. Both of the workers performed this experiment at sodium densities corresponding to large resonance line optical depths. Christoph attempted to allow for this with an optical depth correction corresponding to the path length to the observation window and an attenuation coefficient for lamp radiation measured in another cell. He noted, however, that the measured attenuation coefficient did not agree with a calculated expectation. This could easily be a consequence of the lamp profile or incorrect Na density. But it should be noted that even if the correct optical mean free path were known, the proportion of electron excited resonance radiation escaping an observation window depends on the relative probabilities of diffusion out the observation window versus to other walls or internal surfaces that can absorb the resonance radiation. If the window is closer than most other surfaces and the optics detect radiation from the entire window region then too much rather than too little radiation is detected. Neither Ref. 2 nor 6 attempted to evaluate the actual effect of the resonance radiation diffusion. The geometry of the apparatus in Ref. 6 was decidedly different from that in Ref. 2, whereas Ref. 6 utilized Christoph's optical depth correction verbatim. In addition, it is now well known that glass walls absorb vast quantities of sodium and can thereby prevent the attainment of the saturated vapor pressure, whereas the measurements of Refs. 2 and 6 both assumed the saturated vapor pressure.

References 3–6 also used large electron currents at low energies. This could result in spreading of the electron beam outside the field of view of the detection system so that only a portion of the electron impact radiation was observed. It can also cause space-charge depression of the electron-beam energy and widening of the electron-beam energy distribution. For these reasons we conclude that the normalizations used by both Christoph and Zapesochnyĭ for the resonant transition cross section are not reliable. Note also that if we raise the cross section of Refs. 3–6 to the magnitude of ours the slope of that cross section in the threshold region is still much less than ours. This might be due to the space-charge effects we have discussed.

However, as we mentioned earlier, the nonresonant transition cross sections measured in Ref. 4 may be more accurate. Support for these measurements comes from the recent three- and four-state close-coupling calculations for the $3d$ cross section.[10,11] These results along with the $3d$ cross section given in Ref. 4 are presented in Fig. 5. It is perhaps significant that the larger cascade cross section theoretically indicated at 4 eV would remove most of the 4-eV "hump" in our $3s$-$3p$ cross section and also improve the agreement with theory. The slow rise above threshold of the $3s$-$3p$ cross section from Refs. 3–6 further supports such a correction.

The polarization results of our experiment are given in Figs. 9 and 10 and Table I. Comparison with other experiments (Fig. 9) shows good agreement with Ref. 26 but some difference from Ref. 14. The results of Ref. 14 were extrapolated to obtain a threshold polarization value of $(+14.8 \pm 1.8)\%$, in excellent agreement with the theoretical prediction of $+14.1\%$.[13] We have not attempted an extrapolation of our data to threshold because of large uncertainties below 2.4 eV (see Fig. 10). In this low-energy region, our electron-beam energy distribution was similar to that of Ref. 14 (about $\frac{1}{4}$ eV) while that of Ref. 26 was ~ 70 meV at 2.4 eV and ~ 180 meV for the other energies; hence differences due to smearing of polarization values corresponding to different energy widths is ruled out. If the polarization drops from 14.1 to ~ 11% in a narrow energy range above threshold, as indicated by the close-coupling calculations and the measurements of Ref. 26, our experiment will detect an apparent threshold polarization close to 11%. The rapid rise of the cross section at threshold folded into our electron distribution prevents observation of the larger polarizations.

Comparison of our results with theoretical predictions for the polarization in the low-energy region (< 10 eV) is shown in Fig. 10. Reference 27 is a two-state close-coupling calculation; Ref. 11 includes the $4s$ and $3d$ states. Although including these two additional states has a minor effect on the cross section, they do affect the polarization results significantly, yielding results in better agreement with our experiment.

From our results and those of Gould[26] we conclude that only close-coupling techniques[9–11,27] have succeeded in predicting reasonable values for the cross section and polarization for the $3s$-$3p$ transition in sodium at low electron energies. Vaĭnshteĭn's model gives good cross-section values

for energies >~ 10 eV. The Born cross section for this hydrogenlike atom is not accurate to 1% until energies several hundred times threshold are reached; whereas the Born cross sections for hydrogen are generally considered to be accurate at some 15 times threshold (Fig. 64 of Ref. 1).

---

*Work supported in part by National Science Foundation Grant No. GP-20696.

†Present address: Physics Department, University of Pittsburgh, Pittsburgh, Pa. 15213.

‡Staff Member, Laboratory Astrophysics Division, National Bureau of Standards.

[1]B. S. Moiseiwitsch and S. J. Smith, Rev. Mod. Phys. 40, 238 (1968).

[2]W. Christoph, Ann. Physik 23, 51 (1935).

[3]I. P. Zapesochnyĭ and L. L. Shimon, Opt. i Spektroskopiya 13, 621 (1962) [Opt. Spectry. 13, 355 (1962)].

[4]I. P. Zapesochnyĭ and L. L. Shimon, Opt. i Spektroskopiya 19, 480 (1965) [Opt. Spectry. 19, 268 (1965)].

[5]I. P. Zapesochnyĭ and O. B. Shpenik, Zh. Eksperim. i Teor. Fiz. 50, 890 (1966) [Sov. Phys. JETP 23, 592 (1966)].

[6]J. P. Zapesochnyĭ, High Temp. USSR 5, 6 (1967).

[7]J. T. Jefferies, *Spectral Line Formation* (Blaisdell, Waltham, Mass., 1968), Chaps. 9 and 10.

[8]L. L. Barnes, N. F. Lane, and C. C. Lin, Phys. Rev. 137, A388 (1965).

[9]E. M. Karule and R. K. Peterkop, in *Atomic Collisions*, edited by V. Ya. Veldre (Akademiya Nauk Latvovskoi SSR Institut Fizika, Riga, 1965), Vol. III, p. 3, Translation No. TT-66-12939 available through SLA Translation Center John Crerar Library, Chicago, Ill.

[10]D. F. Korff, S. Chung, and C. C. Lin, Bull. Am. Phys. Soc. 16, 218 (1971); and private communication.

[11]D. L. Moores and D. Norcross, J. Phys. B (to be published).

[12]L. A. Vaĭnshteĭn, V. Opykhtin, and L. Presnyakov, Zh. Eksperim. i Teor. Fiz. 47, 2306 (1964) [Sov. Phys. JETP 20, 1542 (1965)].

[13]D. R. Flower and M. J. Seaton, Proc. Phys. Soc. (London) 91, 59 (1967).

[14]H. Hafner and H. Kleinpoppen, Z. Physik 198, 315 (1967).

[15]E. A. Enemark, thesis (University of Colorado, 1971) (unpublished).

[16]D. W. O. Heddle, Proc. Phys. Soc. (London) 90, 81 (1967).

[17]C. D. Hodgman, R. C. Weast, and S. M. Selby, editors, *Handbook of Chemistry and Physics*, (Chemical Rubber, Cleveland, 1961).

[18]M. Lapp and L. P. Harris, J. Quant. Spectry. Radiative Transfer 6, 169 (1966).

[19]J. A. Simpson, Rev. Sci. Instr. 32, 1283 (1961).

[20]M. I. D'Yakonov and V. I. Perel, Zh. Eksperim. i Teor. Fiz. 47, 1483 (1964) [Sov. Phys. JETP 20, 997 (1965)]; A. Omont, J. Phys. (Paris) 26, 576 (1965).

[21]J. P. Barrat, J. Phys. Radium 20, 541 (1959); 20, 633 (1959); 20, 657 (1959).

[22]I. C. Percival and M. J. Seaton, Phil. Trans. Roy. Soc. London A251, 113 (1958).

[23]S. Geltman, *Topics in Atomic Collision Theory*, (Academic, New York, 1969), Chap. 14.

[24]W. L. Wiese, M. W. Smith, and B. M. Miles, *Atomic Transition Probabilities—Sodium Through Calcium* U. S. Natl. Bur. Std. National Standard Ref. Series—22 (U. S. GPO, Washington, D. C., 1969), Vol. II, p. 2.

[25]H. Kopfermann, *Nuclear Moments* (Academic, New York, 1958), Chap. 1.

[26]G. N. Gould, thesis (University of New South Wales, 1970) (unpublished).

[27]E. M. Karule, J. Phys. B 3, 860 (1970).